FERMILAB-PUB-24-0406-STUDENT
2024 URA-Fermilab Undergraduate Women in STEM
July 29th, 2024

Research Report

Katsuya Yonehara, Fermilab
Sam Zeller, Fermilab

NON-CONTACT REAL-TIME TARGET HEALTH MONITOR

Alanice Agosto Reyes
Accelerator Division
Fermi National Accelerator Laboratory
Batavia, IL 60510

ABSTRACT

This paper presents the results from initial tests and measurements conducted using a newly developed system designed to monitor radiation damage in targets employed in accelerators. This radiation damage is assessed by measuring the reflectivity of S- and P-polarized waves. Constant irradiation to targets can result in internal changes that eventually affect the material's properties, such as optical properties. Hence, due to these radiation-induced alterations, the angle at which S- and P-polarized waves get reflected is expected to change measurably, making it possible to monitor the changes in real time. To achieve this ultimate goal, several small-scale experiments were conducted to ensure that the desired equipment was working properly. In these experiments, instruments like a 635-nm laser, monochromator, polarizer, SiPM, picoammeter, and an integrating sphere were employed. Once every one of these components is tested, reflectivity measurements will be performed using a sample of tungsten, a material often used for the targets. In the future, the system will be implemented in projects like Mu2e, Mu2e-II, LBNF, AMF, and muon colliders. The development of this system presents an innovative idea that will be capable of obtaining this information without the need for direct contact, as opposed to current methods being employed for studies involving radiation damage.

INTRODUCTION

Targets are of common use for accelerator-based facilities performing any type of particle physics experiments. These targets are constantly being bombarded with high-energy particles, which eventually might affect their capabilities. Current methods used to monitor radiation damage typically involve direct contact with the target or complete removal of the system; hence, making them not the most effective methods. For this reason, this group is working on developing a non-contact, non-destructive target health sensor that will be capable of studying this radiation damage at a distance and in real time. This will be done by measuring the reflectivity of S- and P-polarized waves.

To understand how constant radiation exposure affects the reflectivity of S- and P-polarized waves, it is necessary to look first at models used to describe these types of interactions. When radiation strikes the surface of the material, the electric fields from it interact with the electromagnetic fields of the atoms in the material, causing temporal or permanent changes in the arrangement of the atoms. This light-matter interaction is normally described with the Lorentz-Drude model (LD model), which combines two main ideas. The first one comes from the Drude model, which considers only the free electrons in the material. When the surface is irradiated, the electrons move around the medium in response to that alteration, hence changing the material's properties. On the other hand, the Lorentz model considers the bound electrons and views them as oscillators. Irradiating the surface in this case will make those electrons

oscillate back and forth and vibrate at a specific frequency. If the frequency of the incident irradiation matches that of the electrons, resonance is achieved, causing the material to absorb more energy, thereby affecting its reflective and transmission properties. A complete model for the light-matter interaction is obtained when both of these are combined. In the language of physics and mathematics, all of this interaction can be explained with the dielectric function.

$$\hat{\epsilon}_r = 1 - \frac{f_0\,\omega_p^2}{\omega(\omega - i\,\Gamma_0)} + \sum_{i=1}^{m} \frac{f_i\,\omega_p^2}{\omega_i^2 - \omega^2 + i\,\omega\,\Gamma_i}, \qquad (1)$$

This function helps understand how the material responds to electric fields or electromagnetic waves when exposed to them. As can be observed, the function has both a real and imaginary part. The real part describes how the material stores electrical energy, while the imaginary part is related to the energy absorption of the material. This function contains specific parameters that are unique for each material, which can be determined experimentally. It is also possible to relate this function to the refractive index by the following equation:

$$n(\omega) = \sqrt{\varepsilon(\omega)} \qquad (2)$$

Given that the goal of the project is to measure reflectivity, this relation presents a direct way to relate the dielectric function and the reflectivity. For the case of reflectivity, Fresnel's equations help with the understanding of how light reflects between two media with different refractive indexes. These equations are presented below, for the S- and P-polarization respectively.

$$R_s = \left| \frac{n_0 cos(\theta) - n_1 \sqrt{1 - \left(\frac{n_0}{n_1} sin(\theta)\right)^2}}{n_0 cos(\theta) + n_1 \sqrt{1 - \left(\frac{n_0}{n_1} sin(\theta)\right)^2}} \right|^2, \qquad (3)$$

$$R_p = \left| \frac{n_0 \sqrt{1 - \left(\frac{n_0}{n_1} sin(\theta)\right)^2} - n_1 cos(\theta)}{n_0 \sqrt{1 - \left(\frac{n_0}{n_1} sin(\theta)\right)^2} + n_1 cos(\theta)} \right|^2, \qquad (4)$$

Determining the dielectric function might be tedious work; however, the dependence on the incident angle in Fresnel's equations presents an alternative for obtaining this function. At Brewster's angle, the reflectivity of the P-polarization is zero. Therefore, setting the reflectivity for the P-polarized wave to zero will give the refractive index of the medium through the following relation:

$$\tan\theta_B = \frac{n_2}{n_1} \qquad (5)$$

For this project, reflectivity measurements are going to be performed at Brewster's angle using a sample of tungsten (a material often used for targets in accelerators).

NOMENCLATURE

For reference, the following list presents the symbols in all the equations shown in this paper.

R_p	reflectivity of p-polarized wave
R_s	reflectivity of s-polarized wave
f_i	oscillator strength
n_0	refractive index of medium 0
n_1	refractive index of medium 1
Γ_i	damping of the oscillator
ε_r	dielectric function
θ	angle of incidence
θ_B	Brewster's angle
ω	frequency of incident light
ω_i	oscillator frequency
ω_p	plasma frequency

PROCEDURES

Before performing the reflectivity measurements, smaller tests were performed to ensure that the needed equipment was working as expected. The instruments used for these tests were 1) an automated monochromator from Horiba, 2) a power supply, 3) a picoammeter, 4) an oscilloscope, 5) a silicon photomultiplier (SiPM), 6) a 635 nm laser, a polarizer, and an integrating sphere (these last two items are not shown in the figure).

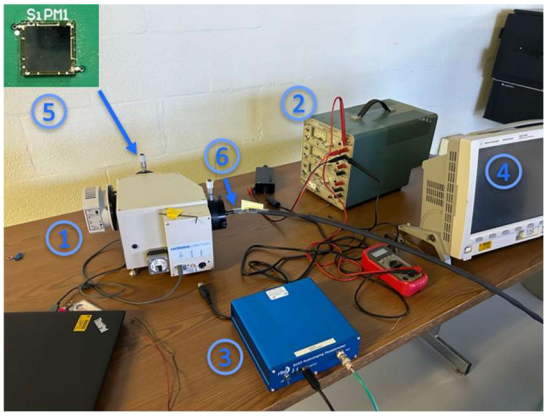

Figure #1: *Experimental setup table with labeled equipment.*

The setup involved directing a 635 nm laser beam onto a monochromator, with a Silicon Photomultiplier (SiPM) placed at a lateral exit of the monochromator to detect this light. The SiPM converts the light signal into a current, which is then measured by a picoammeter. To ensure precise detection, a holder had to be designed to support the SiPM in place at the exit. Given the sensitivity of the SiPM and the need to minimize noise from stray light, the holder was designed to be light-tight.

Using NX Siemens, two designs were created and considered to address this requirement. These designs are shown in Figure #2. In this case, the SiPM was placed in the main part (or "cap") of the holder, and the cylindrical part helped with the shielding of excess light. Both designs share similarities except for the way the main part fits with the cylindrical part; one of them is threaded, while the other one is smooth.

(a)

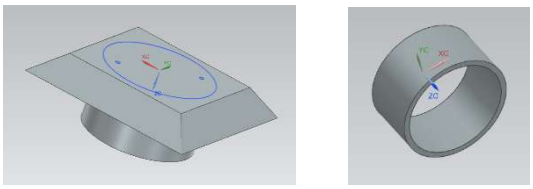

(b)

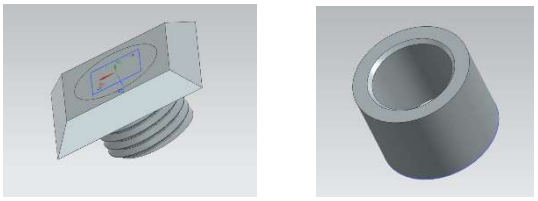

Figure #2: *(a) Shows the first design with the cap/main part and the cylindrical part; (b) shows the second design with the same components.*

After the models were finished, the holder was 3D-printed using Onyx, a nylon-based material reinforced with carbon fiber. This material was chosen in place of the regular PLA due to its darker color, which might help prevent excess light from getting into the system. After printing, four 0.5mm holes were made in the top part of the holder to allow for electrical connections. The SiPM was then soldered, and cables were connected. The result from this is shown in Figure #3.

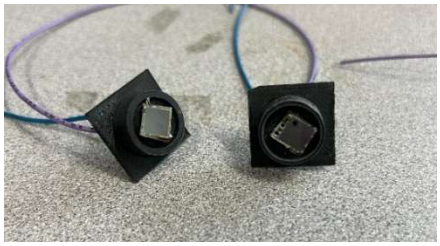

Figure #3: *Printed holders with installed SiPM and electrical connections.*

RESULTS

The result from the SiPM test is shown in Figure #4. The plot displays the relationship between current and wavelength.

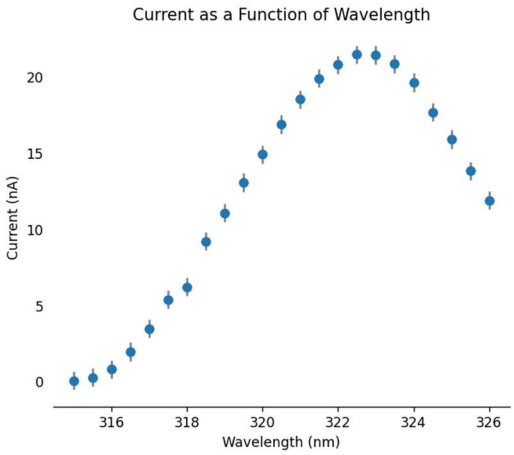

Figure #4: *SiPM response with increased wavelength.*

It is important to note that the monochromator used in this experiment was not calibrated, resulting in a peak at approximately 323 nm rather than the expected 635 nm. Despite this, a visual verification was conducted to confirm that this wavelength corresponds to the 635 nm laser. In addition, the signal obtained was fainter than expected, in the order of nA, as can be seen from the graph.

Reflectivity measurements were successfully conducted, although adjustments were made to the initial setup due to unforeseen issues with the original configuration. Figure #5 illustrates the proposed setup, while Figure #6 displays the revised setup used for these measurements.

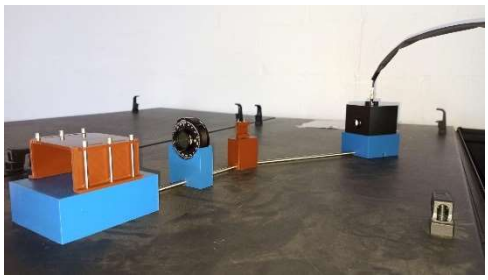

Figure #5: *Shows the proposed setup for the reflectivity measurement. From left to right: laser support, polarizer, sample holder, and integrating sphere.*

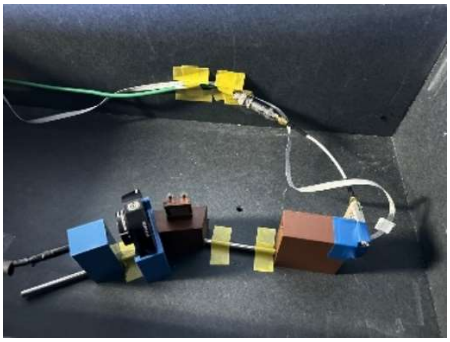

Figure #6: *New reflectivity measurement setup*

Among the modifications made, the new setup does not include the integrating sphere. Previous tests with this instrument did not yield the expected results, and since its function was not critical for the current tests, it was decided to remove it from the setup. Similarly, the original SiPM was replaced with a SiPM with a built-in amplifier, as initial tests indicated that the signal was too weak and could be obscured by background noise. Finally, the instruments were repositioned closer together to minimize the dispersion of laser light. Once the tests were performed, plots were obtained for better visualization of the data, as can be shown in the figures below.

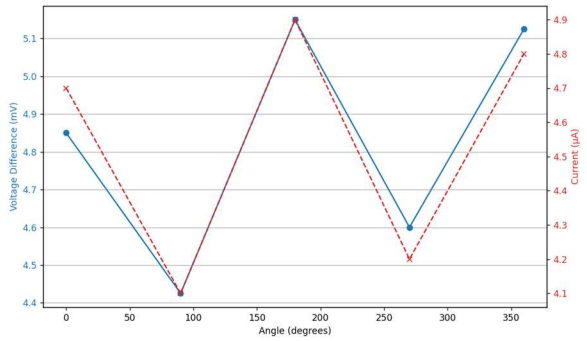

Figure #7: *Shows the voltage difference and current as a function of incident angle, with angle variation starting at 0°.*

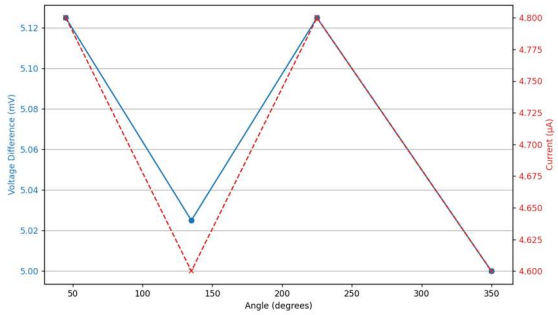

Figure #8: *Shows voltage difference and current as a function of incident angle, with angle variation starting at 45°.*

ANALYSIS AND DISCUSSION

The response of the SiPM was as expected, as shown in Figure #4, confirming that the SiPM is functioning correctly. Regarding the reflectivity measurements, these exhibit the expected behavior and shifts in both current and voltage as the angle of the incident light was varied. The troughs observed represent the minimum values and occur when the reflectivity of the P-polarized wave is zero. The only anomaly noted is in Figure #8, where the changes in current and voltage are minimal; this discrepancy is currently under investigation.

It is important to note that this data pertains solely to a non-irradiated tungsten sample. Future experiments will involve irradiated samples to examine changes in reflectivity, using the results from the non-irradiated sample as a baseline.

In a broader context, theoretical models can generate plots that visualize the expected reflectivity behavior of tungsten under continuous radiation exposure and as a function of wavelength and incident photon energy. These plots, derived from equation (1) and varying different parameters, are presented in Figures #9 and #10.

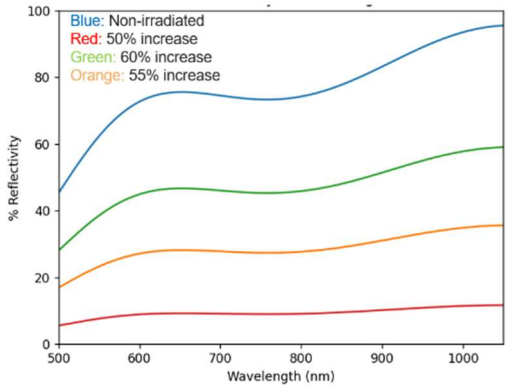

Figure #9: *Expected behavior of the reflectivity of tungsten versus wavelength. This particular graph was obtained by varying the plasma frequency.*

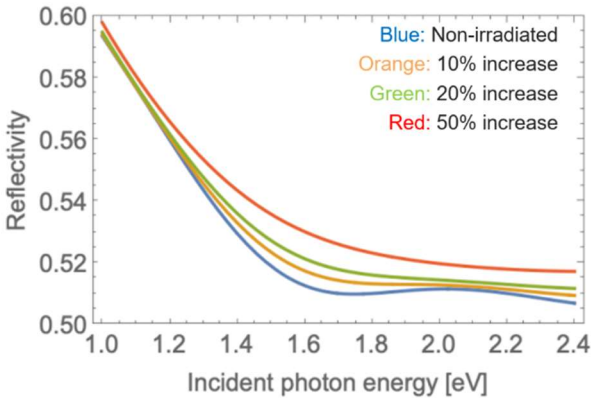

Figure #10: *Estimated reflectivity of tungsten as a function of incident photon energy. This plot was obtained by varying the collision frequency.*

Both graphs illustrate how the material's reflectivity varies with changes in light frequency and exposure. Notably, the plot in Figure #10 was generated by altering the collision frequency. With prolonged radiation exposure, the concentration of free carriers in the material can increase, which in turn raises the collision frequency. The plot in Figure #9, on the other hand, was created by varying the plasma frequency. Since the plasma frequency is influenced by the density of free carriers, any changes in free carrier concentration due to constant radiation exposure are expected to affect the plasma frequency as well.

While these plots provide a clearer understanding of tungsten's expected reflectivity behavior, the actual behavior may differ slightly from predictions. This variation arises because reflectivity depends on numerous variables that can cause deviations from anticipated results. Nonetheless, as illustrated in Figure #10, increased exposure of the target to high-energy radiation leads to more pronounced effects on its reflectivity. These plots are valuable for understanding how constant radiation exposure influences a material's response to light, which can, in turn, impact its performance in the accelerator.

CONCLUSIONS AND SUMMARY

The goal of this project is to advance accelerator target health studies by developing a sensor that assesses radiation damage from continuous exposure. This will be accomplished by measuring the reflectivity of S- and P-polarized waves, which are expected to change due to internal alterations in the targets. Preliminary experiments were conducted to ensure the functionality of the necessary equipment before performing the reflectivity measurements. In these experiments, silicon photomultipliers (SiPMs) were used to capture the signals. Therefore, the first task involved designing a holder for the SiPM. After the design was completed, the SiPM was soldered and placed in a monochromator. Testing of the SiPM confirmed that it was functioning properly. After testing all the equipment, reflectivity measurements were conducted using a non-irradiated tungsten sample, and the results were consistent with expectations. The next steps of the project involve using an irradiated sample to observe the variations in the reflectivity and taking the non-irradiated results as a baseline. Following these measurements, the system will be moved to a larger scale and, in the future, potentially applied to larger projects such as Mu2e, Mu2e-II, LBNF, AMF, and muon colliders.

SCIENCE POLICY STATEMENT

Fermilab’s mission includes leading the world in particle collider experiments. In such experiments, targets are crucial for generating the secondary particles required. However, these targets have a limited lifespan that can be significantly affected by radiation damage if not properly monitored. Accurate assessment of this damage is essential to ensure the longevity and effectiveness of the targets. Therefore, the development of advanced technologies and sensors to monitor radiation damage is critical to achieving Fermilab's mission. By creating innovative, non-contact, non-destructive methods for assessing target health, Fermilab can enhance the precision and reliability of its experiments.

Additionally, compliance with policy acts such as the Atomic Energy Act is important. This act requires the proper management of radioactive sources. Developing and implementing a sophisticated system to monitor radiation damage aligns with these regulations by ensuring the safe and effective handling of radiation sources. Given the target's constant exposure to high-energy radiation, the safest way to monitor and study radiation damage will be from afar, without exposing any personnel to this radiation source. By integrating this non-contact and non-destructive monitoring system, Fermilab will contribute to both the advancement of particle physics and the responsible management of radioactive materials.

ACKNOWLEDGMENTS

This manuscript has been authored by Fermi Research Alliance, LLC under Contract No. DE-AC02-07CH11359 with the U.S. Department of Energy, Office of Science, Office of High Energy Physics.

REFERENCES

Fermilab, 19 January 2024, https://www.fnal.gov/pub/about/index.html. Accessed 28 July 2024

Marco Minissale, Cédric Pardanaud, Régis Bisson, Laurent Gallais. “The temperature dependence of optical properties of tungsten in the visible and near-infrared domains: an experimental and theoretical study.” Journal of Physics D: Applied Physics, 2017, 50 (45), 10.1088/1361-6463/aa81f3. hal-01690700.

Tom Carver, “Atomic Energy Act and Related Legislation”, https://www.energy.gov/ehss/atomic-energy-act-and-related-legislation. Accessed 27 July 2024.